Report

ISSCR

OPEN ACCESS

Xeno-Free and Defined Human Embryonic Stem Cell-Derived Retinal Pigment Epithelial Cells Functionally Integrate in a Large-Eyed Preclinical Model

Alvaro Plaza Reyes,[1,5] Sandra Petrus-Reurer,[1,2,5] Liselotte Antonsson,[1] Sonya Stenfelt,[1] Hammurabi Bartuma,[2] Sarita Panula,[1] Theresa Mader,[1] Iyadh Douagi,[3] Helder André,[2] Outi Hovatta,[1,4,6] Fredrik Lanner,[1,6,*] and Anders Kvanta[2,6]

[1]Department of Clinical Sciences, Intervention and Technology, Karolinska Institutet, 14186 Stockholm, Sweden
[2]Department of Clinical Neuroscience, Section for Ophthalmology and Vision, St. Erik Eye Hospital, Karolinska Institutet, 11282 Stockholm, Sweden
[3]Department of Medicine, Center for Hematology and Regenerative Medicine, Karolinska Institutet, 14157 Stockholm, Sweden
[4]Cell Therapy Department, Nova Southeastern University, Fort Lauderdale, FL 33314, USA
[5]Co-first author
[6]Co-senior author
*Correspondence: fredrik.lanner@ki.se
http://dx.doi.org/10.1016/j.stemcr.2015.11.008

SUMMARY

Human embryonic stem cell (hESC)-derived retinal pigment epithelial (RPE) cells could replace lost tissue in geographic atrophy (GA) but efficacy has yet to be demonstrated in a large-eyed model. Also, production of hESC-RPE has not yet been achieved in a xeno-free and defined manner, which is critical for clinical compliance and reduced immunogenicity. Here we describe an effective differentiation methodology using human laminin-521 matrix with xeno-free and defined medium. Differentiated cells exhibited characteristics of native RPE including morphology, pigmentation, marker expression, monolayer integrity, and polarization together with phagocytic activity. Furthermore, we established a large-eyed GA model that allowed in vivo imaging of hESC-RPE and host retina. Cells transplanted in suspension showed long-term integration and formed polarized monolayers exhibiting phagocytic and photoreceptor rescue capacity. We have developed a xeno-free and defined hESC-RPE differentiation method and present evidence of functional integration of clinically compliant hESC-RPE in a large-eyed disease model.

INTRODUCTION

Age-related macular degeneration (AMD), the most common cause of severe vision loss in the Western world, occurs in wet (neovascular) and dry (degenerative) forms. In early dry AMD, the retinal pigment epithelium (RPE) becomes dysfunctional, whereas end-stage disease, geographic atrophy (GA), is characterized by degeneration of RPE and photoreceptors (Bhutto and Lutty, 2012). The RPE is a monolayer of polarized cells that constitutes the outer blood-retina barrier and performs central tasks in the eye, e.g., light adsorption, secretion of growth factors, and phagocytosis of photoreceptor outer segments (POS) (Sparrow et al., 2010). The apical surface harbors microvilli that interact with the light-sensitive POS, whereas the basolateral surface adheres to Bruch's membrane (BM), which in turn separates the RPE from the underlying choroid. Subretinal transplantation of RPE cells derived from human embryonic stem cells (hESC) could potentially be used as replacement therapy in GA (Schwartz et al., 2012, 2015). However, a critical question is whether donor cells integrate into the host RPE and support the overlying photoreceptors. Experimental transplantations of hESC-RPE have only been conducted in small-eyed rodent models (Carido et al., 2014; Idelson et al., 2009; Lund et al., 2006; Vugler et al., 2008). Functional effects in these models are however non-specific and surgical techniques, instrumentation, and imaging methods differ from those applied in humans, limiting their use as preclinical models (e.g., Pinilla et al., 2009). We have recently described a damage model in the large-eyed rabbit that exhibits typical GA changes including photoreceptor loss and RPE alterations (Bartuma et al., 2015).

Several hESC-RPE derivation protocols have been described with the common limitation of relying on culture steps that involve xeno- or human-feeder cells or use medium components that are either undefined or not xeno-free (Klimanskaya et al., 2004; Lane et al., 2014; Osakada et al., 2009; Pennington et al., 2015; Vaajasaari et al., 2011). Recently, we described a defined and xeno-free clonal culture of hESC using recombinant human laminin (rhLN) and E-cadherin (Rodin et al., 2014a, 2014b). Encouraged by this work, we set out to evaluate whether rhLN-matrix could support efficient hESC-RPE differentiation. BM, the RPE basement membrane, contains four LNs, LN-111, LN-332, LN-511, and LN-521, that adhere to the RPE via specific integrins (Aisenbrey et al., 2006).

In the present study, we show that rhLNs are more effective in supporting xeno-free and defined differentiation compared with exogenous matrix such as gelatin, used in
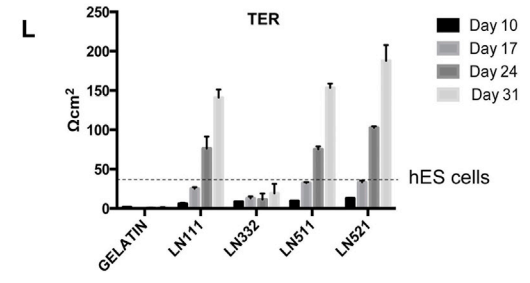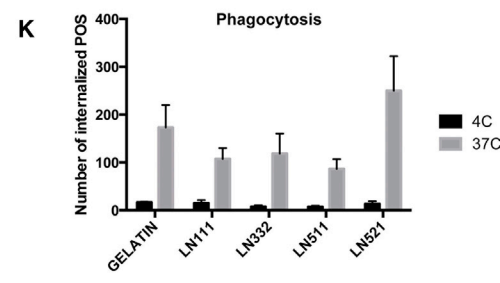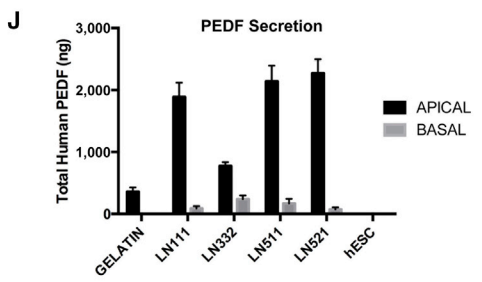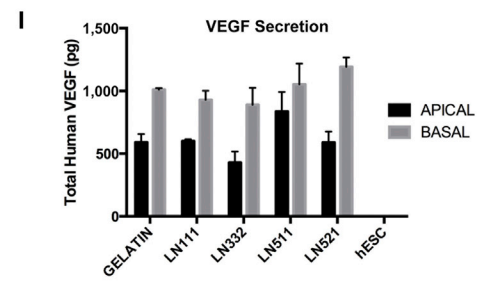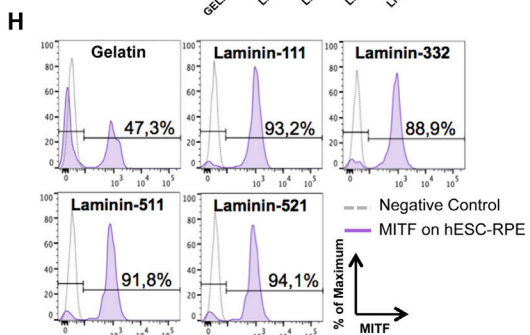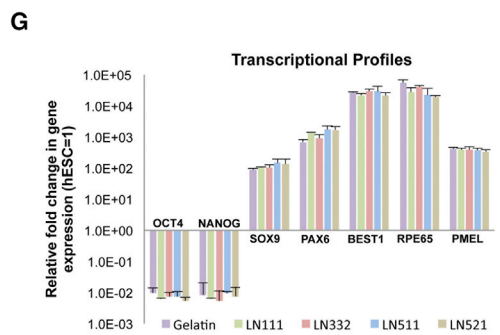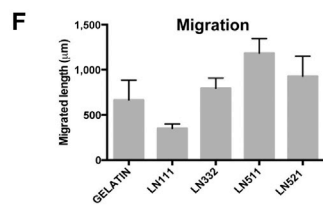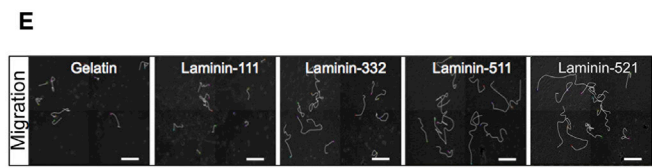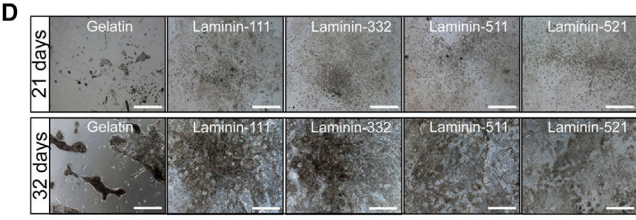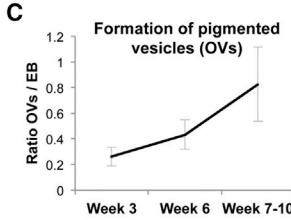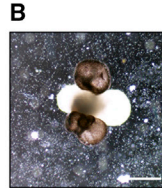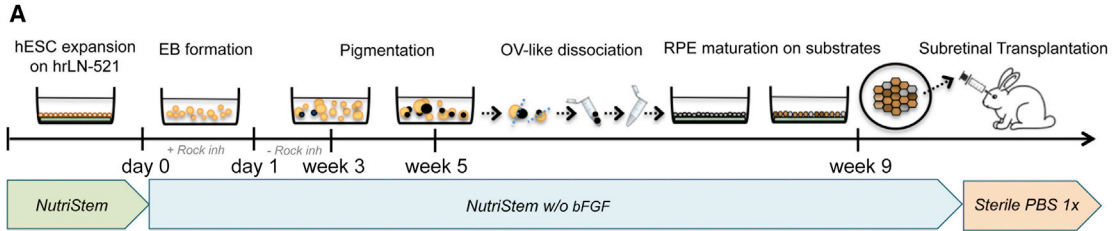
(legend on next page)

ongoing clinical studies (Schwartz et al., 2012). Moreover, we demonstrate that suspension transplantations of rhLN-521-hESC-RPE integrate as polarized subretinal monolayers that rescue overlying photoreceptors from induced damage. We conclude that rhLN-521 effectively supports differentiation of clinically compliant hESC-RPE, and presents evidence of efficient long-term functional integration of hESC-RPE in a large-eyed disease model.

RESULTS

Robust Induction of Primary Pigmented Cells Using Suspension Differentiation in Defined Medium

We have recently developed a xeno-free hESC derivation and culture methodology, using rhLN-521-based matrix and a xeno-free and defined NutriStem hESC XF medium containing basic fibroblast growth factor (bFGF) (Rodin et al., 2014a, 2014b). As FGF removal is critical for RPE differentiation (Pittack et al., 1997), we decided to evaluate whether our hESC culture methodology could efficiently support hESC-RPE differentiation following bFGF removal.

hESCs were cultured on rhLN-521 and manually scraped to produce a suspension culture of embryoid bodies (EBs) in NutriStem hESC XF without bFGF (Figures 1A and 1B). This culture robustly supported formation of pigmented structures resembling optical vesicles (OVs) at as early as 3 weeks of differentiation (Figures 1A and 1B). At this stage, we observed an average of 0.3 OVs per EB, which in the subsequent weeks increased to 0.8 per EB (Figure 1C). This efficiency of OV induction is well in line with previous reports (Idelson et al., 2009), confirming that our xeno-free culture medium efficiently supports the first stage of hESC-RPE differentiation.

rhLN-521 Efficiently Supports Homogeneous Expansion of Pigmented and Functional hESC-RPE

Endogenous BM contains four LNs: LN-111, LN-332, LN-511, and LN-521. Consequently, we decided to compare subsequent expansion and maturation of primary pigmented cells on gelatin or rhLNs found in the endogenous BM.

The pigmented OVs were mechanically cut out using a scalpel and dissociated into single cells. Cells were seeded through a cell strainer onto gelatin or LN-coated dishes. Three days following plating, it was clearly observable that LN-521 had the best performance, with 69% plating efficiency compared with 8% in gelatin-coated cultures (Table S1). Pigmentation was initially lost in all cultures, but was progressively reestablished from day 21 (Figure 1D), as previously described. Interestingly, time-lapse microscopy showed that cells on rhLN-511 and rhLN-521 were highly migratory forming uniform monolayers throughout the wells (Figures 1D–1F and Movie S1), while progressively maturing into pigmented hexagonal cells. This correlates well with a previous study showing that the same subtype of integrin receptors recognizes LN-511 and LN-521 (Aisenbrey et al., 2006). Cells on gelatin were migratory, but tended to stay in tight colonies and failed to fully cover the plate even after 77 days (Figures 1D–1F and S1A).

Transcriptional analysis showed similar profiles in hESC-RPE differentiated on each of the five substrates with

Figure 1. Xeno-Free and Defined RPE Differentiation of hESC to hESC-RPE

(A) Differentiation protocol scheme. Confluent hESC cultures were scraped and cultured in low-attachment plates with NutriStem −/− (bFGF removed) to form EBs with Rock inhibitor during the first 24 hr. First pigmentation (OV-like structures) appears following week 3. At week 5, pigmented structures are cut out with a scalpel and dissociated into single cells. Cells are plated on different substrates and cultured until homogeneous pigmentation is reached (week 9). RPE cells are dissociated to a single-cell suspension for subretinal injection in the rabbit eye.

(B) hESC-EB with pigmented OV-like structures.

(C) Quantification of pigmented OV formation per starting EB during differentiation. Bars represent means ± SD from three independent experiments.

(D) Differentiation on gelatin and LN-111, LN-332, LN-511, and LN-521 following 21 and 32 days. See also Movie S1.

(E) Images depicting the migratory tracks of ten random cells during the first 7 days of culture on the different conditions.

(F) Bar graph showing the average length migrated by cells growing on the different substrates. Three individual wells with ten cells analyzed in each were quantified over a period of 7 days using time-lapse imaging. Bars represent means ± SD.

(G) Transcriptional analysis of hESC-RPE differentiated on the different substrates. Values are normalized to *RPLPO* and *GAPDH* and displayed as relative to undifferentiated hESCs. Bars represent means ± SEM from three independent experiments.

(H) Flow cytometry analysis of MITF expression on hESC-RPE cells grown on the different substrates for 29 days.

(I and J) Polarized secretion of VEGF and PEDF in hESC-RPE. Bars represent means ± SEM from three independent experiments.

(K) Phagocytosis of fluorescein isothiocyanates (FITC)-labeled POS by hESC-RPE on the different substrates. hESC-RPE cells incubated with FITC-labeled POS at 4°C were used as negative controls. Bars represent means ± SD from three independent experiments.

(L) TER measurements of hESC-RPE cells grown on the different substrates. The TER value for undifferentiated hESCs (fully confluent plate) is shown for comparison (dashed line). Bars represent means ± SEM from three independent experiments.

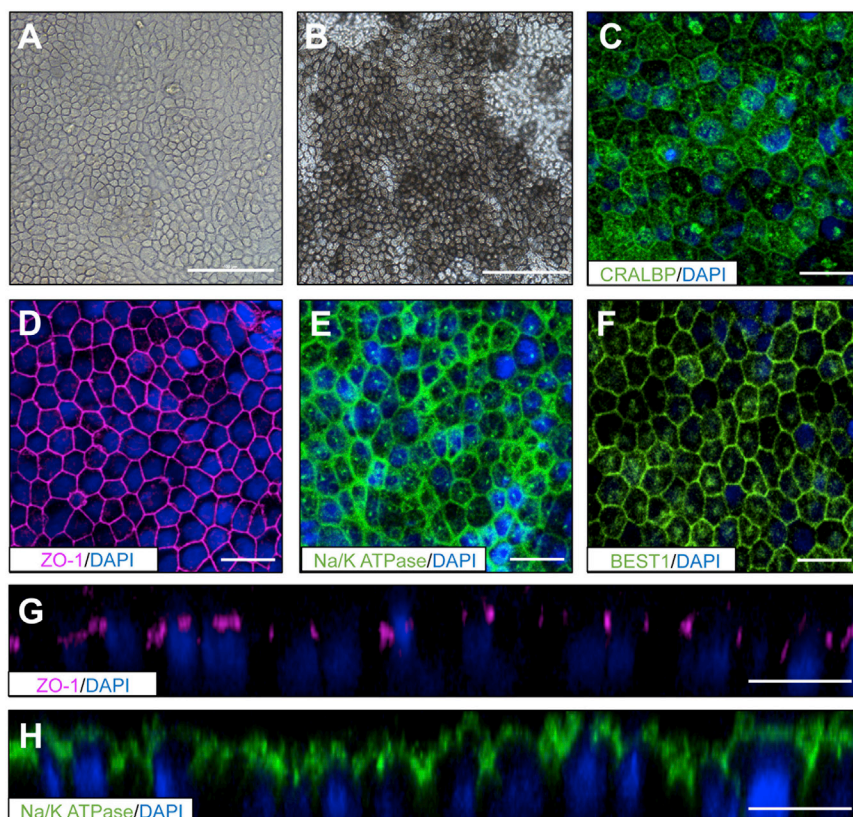Scale bars: B, D, E, 500 μm.

See also Figure S1.

Figure 2. Morphology and Marker Expression of rhLN-521-hESC-RPE

(A) Bright-field image of hESC-RPE cells grown on rhLN-521 acquiring hexagonal shape before pigmentation.

(B) Mature and highly pigmented hESC-RPE cells displaying hexagonal morphology.

(C–F) Expression of key RPE markers: cellular retinaldehyde-binding protein (CRALBP), zonula occludens protein-1 (ZO-1), Na/K-ATPase, and Bestrophin1 (Best1) by immunostaining.

(G and H) Z-stack confocal projections showing polarized expression of ZO-1 and Na/K-ATPase markers on the apical side of the hESC-RPE.

Scale bars: A, B, 100 μm; C–H, 20 μm.

reduction of pluripotency-associated transcripts *OCT3/4* and *NANOG*, together with robust expression of neuroectoderm transcripts sex-determining region Y-box 9 protein (*SOX9*) and paired box 6 (*PAX6*). Low expression levels of paired box 3 (*PAX3*) and endothelin receptor B (*EDNRB*) transcripts eliminated the possibility of contaminating melanocytes in any of the substrates (Figure S1B). RPE differentiation was evident with expression of bestrophin 1 (*BEST1*), RPE-specific protein 65 kDa (*RPE65*), and premelanosome protein (*PMEL*) (Figure 1G). However, more sensitive single-cell analysis of mature RPE purity through flow cytometry for microphthalmia-associated transcription factor (MITF) and BEST1 showed more homogeneous expression on all LNs compared with gelatin (Figures 1H and S1C).

Functionally, all cultures showed polarized secretion of vascular endothelial growth factor (VEGF) and pigment epithelium-derived factor (PEDF), as well as active phagocytosis of POS (Figures 1I–K and S1D–S1G). hESC-RPE only secreted PEDF from week 5 and not earlier (data not shown). We found that hESC-RPE growing on LN-332 and gelatin displayed lower levels of PEDF secretion compared with those growing in all the other tested conditions. Also, interestingly, transepithelial electrical resistance (TER) measurements proved the functional tight junction integrity of our hESC-RPE monolayer on LN-111, LN-511, and LN-521 in a time-dependent manner, but not on LN-332 and gelatin (Figure 1L). This observation is in line with the fact that RPE cells did not manage to form a continuous monolayer when growing on these two substrates (Figures 1D and S1A). hESC-RPE seeded on LN-521 reached values of 180 Ω cm^2 after 31 days, indicative of a functionally mature monolayer. Extended analysis confirmed that rhLN-521-hESC-RPE cultures acquired a pigmented and hexagonal morphology (Figures 2A and 2B), and they were also shown to be uniformly positive for cellular retinaldehyde-binding protein (CRALBP) and BEST1 with clear apical polarization of zonula occludens protein 1 (ZO-1) and Na/K-ATPase (Figures 2C–2H).

hESC-RPE Transplantation into Albino Rabbits

For transplantation, we chose the albino rabbit with an eye size approximately 70% of that the human eye. All major retinal and subretinal layers were clearly detectable using cross-sectional spectral domain optical coherence tomography (SD-OCT) (Figures S2A and S2B).

We next transplanted suspensions of rhLN-521-hESC-RPE into the subretinal space. Pigmentation was not evident by ophthalmoscopy but a thickened and irregular RPE/BM layer was detected by SD-OCT 1 week after
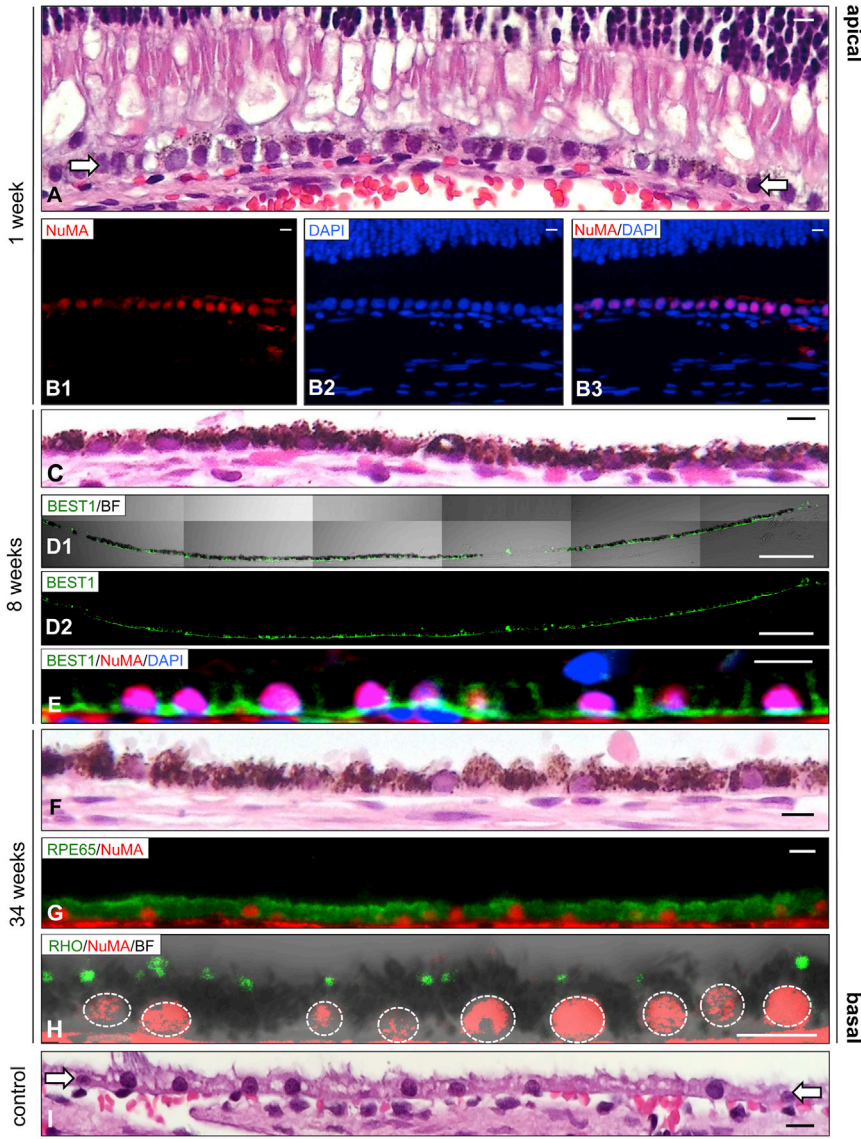
Figure 3. In Vivo Integration of rhLN-521-hESC-RPE

(A) H&E-stained section 1 week after transplantation demonstrates the presence of lightly pigmented cells as a continuous monolayer (arrows) between the POS and the underlying choriocapillaris.

(B) Subretinal human (NuMA-positive) cells detected in the injected region. Panels show NuMA (B1), DAPI (B2) and NuMA with DAPI (B3).

(C) A heavily pigmented subretinal monolayer of transplanted cells is detected in the injected region 8 weeks after transplantation.

(D and E) 8 weeks after transplantation, the integrated NuMA-positive rhLN-521-hESC-RPE cells are polarized with basolateral BEST1 expression. BF, bright field. Panels show BEST1 with BF (D1) and BEST1 only (D2).

(F–H) 34 weeks after transplantation, a heavily pigmented monolayer is present in the injected region displaying RPE65-positive cells and engulfment of rhodopsin-positive particles. Dashed lines represent individual nuclei.

(I) The non-pigmented native RPE layer (arrows) of an untreated area is shown for comparison.

Scale bars: A–C, 10 μm; D, 100 μm; E–I, 10 μm.

transplantation (Figure S2C). Histologic analysis demonstrated a monolayer of lightly pigmented cells that integrated into the host RPE overlaid by well-preserved photoreceptors (Figure 3A). Positive immunostaining for human nuclear mitotic apparatus protein (NuMA) confirmed the human origin of the cells (Figure 3B). Eight weeks after transplantation, monolayers of cells had become heavily pigmented and acquired a polarized phenotype as demonstrated by basolateral expression of BEST1 in the injected area (Figures 3C–3E and S2E). Importantly, all NuMA-positive cells were also pigmented and BEST1-positive. Pigmented rhLN-521-hESC-RPE monolayers with preservation of the neurosensory retina were further observed for up to 34 weeks (Figures 3F, S2C, and S2D). Donor cells were positive for the specific RPE marker RPE65 and cyto-

plasmic rhodopsin suggestive of maintained phagocytic activity (Figures 3G and 3H).

In Vivo Photoreceptor Rescue by hESC-RPE

In the albino rabbit, subretinal injection of PBS alone creates a GA-like phenotype including photoreceptor loss (Bartuma et al., 2015). We therefore tested whether transplanted rhLN-521-hESC-RPE possessed photoreceptor rescue capacity. The outer nuclear layer (ONL), normally consisting of five to six layers, was reduced to a single layer in PBS-injected eyes (Figure 4A), whereas eyes transplanted with rhLN-521-hESC-RPE had preserved ONL and POS (Figure 4B). Integration of transplanted cells was further necessary for ONL rescue as outer retinal thickness (ORT) measurements in eyes with minimal or no integration were
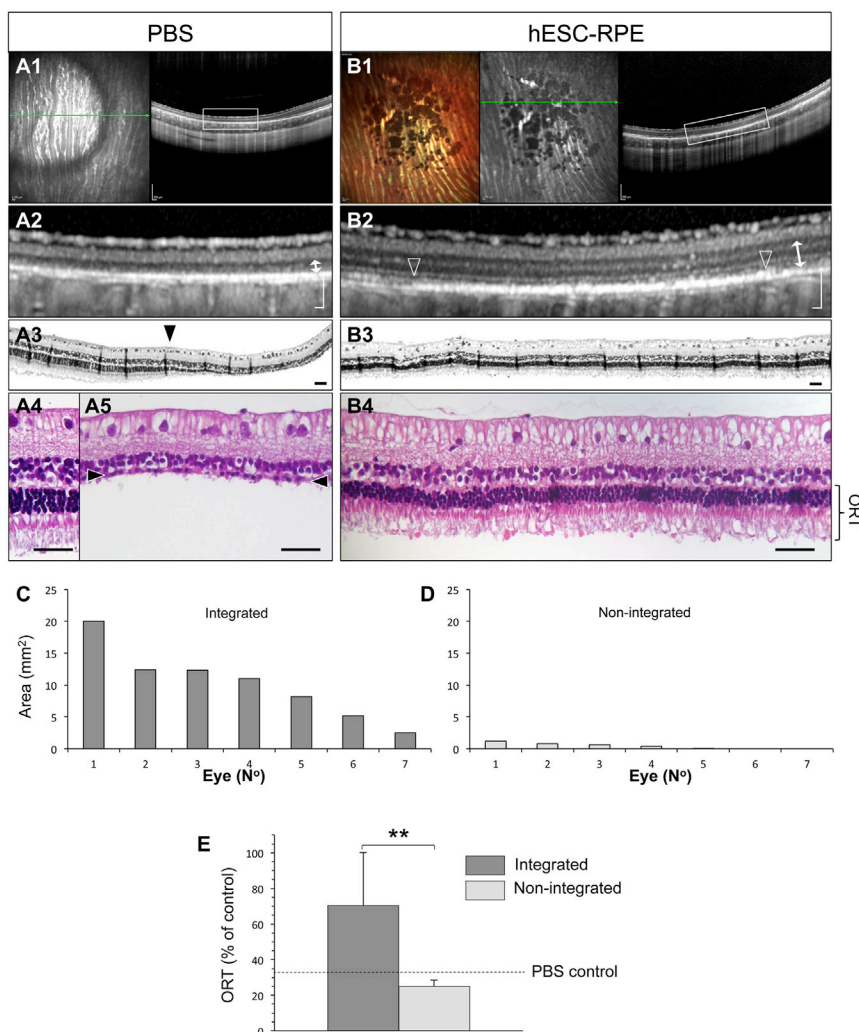
Figure 4. Photoreceptor Rescue by Transplanted rhLN-521-hESC-RPE

(A) PBS-induced photoreceptor degeneration is shown as a hyperreflective circle and outer retinal thinning by infrared-confocal scanning laser ophthalmoscopy (A1) and SD-OCT (A2) respectively. Green arrow, SD-OCT scan plane. A H&E stained section of the bleb transition zone (arrowhead, A3) is shown with the normal (A4) and degenerated (arrowheads, A5) photoreceptor layer magnified. ORT is indicated (arrow).

(B) Two months after transplantation, large pigmented areas are shown (B1) with integrated rhLN-521-hESC-RPE shown as a hyperreflective band (between arrowheads, B2). The overlying neurosensory retina is well preserved as demonstrated by SD-OCT (B2) and histology (B3, B4). ORT is indicated (arrow).

(C–E) ORT is significantly greater in eyes with integrated (defined as a pigmented area >2.5 mm^2) than with non-integrated (defined as a pigmented area <2.5 mm^2) rhLN-521-hESC-RPE. The ORT for PBS injection alone is adapted from Bartuma et al. (2015) and shown for comparison (dashed line, E). Bars represent means ± SD from 14 injected eyes. See also Supplemental Experimental Procedures.

Scale bars: A1, A2, B1, B2, 200 μm; A3, A4, A5, B3, B4, 50 μm. **p < 0.01 (2-sided Student's t test).

See also Figures S2 and S3.

similar to those with PBS treatment alone (Figures 4C–4E). Importantly, undifferentiated hESCs and fibroblasts that formed transient cell aggregates were not protective of photoreceptor loss (Figures S3A and S3B). Thus, the photoreceptor rescue model showed evidence of both specificity (i.e., non-RPE cells were ineffective) and sensitivity (i.e., only integrated RPE cells were effective) for functional RPE.

DISCUSSION

Our differentiation method based on rhLN-521 completely eliminates undefined and animal-based products throughout the process from derivation of hESCs to differentiated functional hESC-RPE. Using our approach, we can avoid microbial contamination, including new agents that have not yet been identified. In addition, we can prevent the identified risk of rejection potentially brought by non-human proteins into the cells during culture and/or differentiation (Aisenbrey et al., 2006). Key to our methodology is the combined use of xeno-free and defined culture medium with a relevant extracellular matrix. BM supporting the RPE contains collagen types I, II, and IV, fibronectin, heparin sulfate proteoglycans, and LNs: LN-111, LN-332, LN-511, and LN-521 (Campochiaro et al., 1986; Martin et al., 2005). As recombinant mouse LN-111 has been shown to support RPE differentiation (Rowland et al., 2013) and we have shown that LN-521 supports derivation and culture of hESCs (Rodin et al., 2014b), we set out to evaluate LNs in a xeno-free and defined differentiation to functional RPE. In accordance with previous observations, we found that rhLN-511 and rhLN-521 supported the highest degree of migration (Aisenbrey et al., 2006), which allowed the cells to spread out evenly in the culture plates. Interestingly, TER assessment from human adult retinal explants and immortalized RPE cell lines has been

reported to reach 148 and 100 Ω cm^2, respectively ([Hornof et al., 2005](#)). In our culture, cells seeded on LN111, LN511, and especially on LN521 appear to be as good as human eye explants and superior to immortalized RPE cell lines in creating highly polarized monolayers. Gelatin-coated cultures instead generated tight and irregularly shaped colonies, which failed to fully cover the plate and displayed a poor monolayer functional integrity. All substrates generated cells with similar transcriptional in vitro profiles, but single-cell analysis of MITF and BEST1 revealed significant heterogeneity in gelatin cultures compared with all LN cultures. Expanding cells in suboptimal culture conditions have the inherent risk of selecting for growth-promoting genetic abnormalities. It was therefore encouraging that seeding efficiency on rhLN-521 was 69%, compared with 8% on gelatin. From these in vitro observations, we conclude that rhLN-521 not only eliminates the need for undefined or xeno-derived matrix components but is in fact a more supportive and suitable culture matrix for hESC-RPE.

Upon transplantation, integrated cells initially displayed reduced pigmentation, which was progressively reestablished, similar to what was observed during in vitro hESC-RPE derivation. Concomitantly, integration of donor cells varied both between animals and between eyes of the same animal. A putative explanation is xeno-graft rejection, as failure of integration correlated with signs of immunoreaction including subretinal cell infiltration, retinal atrophy, and donor cell loss. Optimization of our immunosuppressive protocol may thus overcome this variation. In addition, integration may depend on the state of the native RPE as transplanted cells could adhere better to a denuded BM as shown in mice with sodium iodate-induced RPE atrophy ([Carido et al., 2014](#)). Accordingly, we have shown that subretinal injection alone causes disturbed RPE morphology and partial RPE loss ([Bartuma et al., 2015](#)).

In this study, we transplant hESC-RPE to a large-eyed animal. Human and rabbit eyes are of similar size, the main advantage compared with previously studied mouse and rat models ([Carido et al., 2014; Lund et al., 2006](#)). Transplantation in rodents requires high cell concentrations (i.e., typically 50,000 cells/μl or more) and a transscleral approach through the choroid ([Vugler et al., 2008](#)). The outer blood-retinal barrier is thus compromised, potentially triggering an inflammatory response. Moreover, high cell concentrations and limited surgical control may cause misdirection, multilayering, and clumping of transplanted cells. Indeed, several publications have shown that photoreceptor rescue is neither RPE specific nor correlated with an intact donor cell layer (eg. [Pinilla et al., 2009](#)). The large-eyed rabbit allowed us to perform a surgical technique with instrumentation identical to a clinical setting ([el Dirini et al., 1992](#)). The model also permitted high-reso-

lution in vivo tracking of transplanted cells and monitoring of the overlying neurosensory retina through time. Using this methodology, we demonstrated subretinal monolayers of rhLN-521-hESC-RPE that remained for up to 8 months. Furthermore, integrated cells possessed in vivo functionality including phagocytic activity and rescue of photoreceptors from induced degeneration. Importantly, this effect showed both specificity and sensitivity as non-RPE and non-integrated RPE cells were ineffective.

Suspension transplants have been frequently used in rodent models ([Carido et al., 2014; Idelson et al., 2009; Lund et al., 2006; Vugler et al., 2008](#)) and ongoing clinical studies ([Schwartz et al., 2012, 2015](#)). Concerns about this delivery method were raised with the main criticism being possible multilayering of donor cells leading to inefficient integration ([Schwartz et al., 2012](#)). As an alternative, transplantation of cells as prepolarized sheets with or without a supporting biomatrix has been suggested ([Diniz et al., 2013; Stanzel et al., 2014](#)). However, these large transplants are surgically demanding and may lead to retinal scarring and outer retinal degeneration ([Kamao et al., 2014; Stanzel et al., 2014](#)). In the present study, we noted minimal retinal scarring and a well-preserved neurosensory retina overlying the transplanted monolayer. Moreover, by using suspension transplants, we obtained monolayers up to ten times the size of RPE sheets with a typical size of 2–2.5 mm^2 ([Kamao et al., 2014; Stanzel et al., 2014](#)). We demonstrate that a minimally invasive surgical procedure in a large-eyed disease model can achieve high-yield functional long-term hESC-RPE integration with photoreceptor preservation. These findings have important implications for ongoing and future clinical studies for the development of a safe and efficient cell replacement therapy for GA.

EXPERIMENTAL PROCEDURES

Cell Culture and Differentiation
hES line HS980 was established and cultured under xeno-free and defined conditions on rhLN-521, and passaged as previously described ([Diniz et al., 2013; Rodin et al., 2014b](#)). For differentiation, cells were scraped and cultured in low-attachment plates, 5–7 × 10^4 cells/cm^2 in custom-made NutriStem hESC XF medium without bFGF and transforming growth factor β. Rho-kinase inhibitor was included during the first 24 hr. Following differentiation, pigmented areas were cut out using a scalpel, dissociated, passed through a 20G needle, and plated at a density of 0.6–1.2 × 10^4 cells/cm^2.

Subretinal Transplantation and In Vivo Imaging
Dissociated hESC-RPE cells were injected (50 μl, 50,000 cells) subretinally using a transvitreal pars plana technique. SD-OCT and confocal scanning laser ophthalmoscopy was performed to obtain

horizontal cross-sectional b scans and en face fundus in vivo images, respectively.

SUPPLEMENTAL INFORMATION

Supplemental Information includes Supplemental Experimental Procedures, three figures, one table, and one movie and can be found with this article online at http://dx.doi.org/10.1016/j.stemcr.2015.11.008.

AUTHOR CONTRIBUTIONS

ACKNOWLEDGMENTS

REFERENCES

Aisenbrey, S., Zhang, M., Bacher, D., Yee, J., Brunken, W.J., and Hunter, D.D. (2006). Retinal pigment epithelial cells synthesize laminins, including laminin 5, and adhere to them through alpha3- and alpha6-containing integrins. Invest. Ophthalmol. Vis. Sci. 47, 5537–5544.

Bartuma, H., Petrus-Reurer, S., Aronsson, M., Westman, S., André, H., and Kvanta, A. (2015). In vivo imaging of subretinal bleb-induced outer retinal degeneration. Invest. Ophthalmol. Vis. Sci. 56, 2423–2430.

Bhutto, I., and Lutty, G. (2012). Understanding age-related macular degeneration (AMD): relationships between the photoreceptor/retinal pigment epithelium/Bruch's membrane/choriocapillaris complex. Mol. Aspects Med. 33, 295–317.

Campochiaro, P.A., Jerdon, J.A., and Glaser, B.M. (1986). The extracellular matrix of human retinal pigment epithelial cells in vivo and its synthesis in vitro. Invest. Ophthalmol. Vis. Sci. 27, 1615–1621.

Carido, M., Zhu, Y., Postel, K., Benkner, B., Cimalla, P., Karl, M.O., Kurth, T., Paquet-Durand, F., Koch, E., Munch, T.A., et al. (2014). Characterization of a mouse model with complete RPE loss and its use for RPE cell transplantation. Invest. Ophthalmol. Vis. Sci. 55, 5431–5444.

Diniz, B., Thomas, P., Thomas, B., Ribeiro, R., Hu, Y., Brant, R., Ahuja, A., Zhu, D., Liu, L., Koss, M., et al. (2013). Subretinal implantation of retinal pigment epithelial cells derived from human embryonic stem cells: improved survival when implanted as a monolayer. Invest. Ophthalmol. Vis. Sci. 54, 5087–5096.

el Dirini, A.A., Wang, H.M., Ogden, T.E., and Ryan, S.J. (1992). Retinal pigment epithelium implantation in the rabbit: technique and morphology. Graefes Arch. Clin. Exp. Ophthalmol. 230, 292–300.

Hornof, M., Toropainen, E., and Urtti, A. (2005). Cell culture models of the ocular barriers. Eur. J. Pharm. Biopharm. 60, 207–225.

Idelson, M., Alper, R., Obolensky, A., Ben-Shushan, E., Hemo, I., Yachimovich-Cohen, N., Khaner, H., Smith, Y., Wiser, O., Gropp, M., et al. (2009). Directed differentiation of human embryonic stem cells into functional retinal pigment epithelium cells. Cell Stem Cell 5, 396–408.

Kamao, H., Mandai, M., Okamoto, S., Sakai, N., Suga, A., Sugita, S., Kiryu, J., and Takahashi, M. (2014). Characterization of human induced pluripotent stem cell-derived retinal pigment epithelium cell sheets aiming for clinical application. Stem Cell Rep. 2, 205–218.

Klimanskaya, I., Hipp, J., Rezai, K.A., West, M., Atala, A., and Lanza, R. (2004). Derivation and comparative assessment of retinal pigment epithelium from human embryonic stem cells using transcriptomics. Cloning Stem Cells 6, 217–245.

Lane, A., Philip, L.R., Ruban, L., Fynes, K., Smart, M., Carr, A., Mason, C., and Coffey, P. (2014). Engineering efficient retinal pigment epithelium differentiation from human pluripotent stem cells. Stem Cells Transl. Med. 3, 1295–1304.

Lund, R.D., Wang, S., Klimanskaya, I., Holmes, T., Ramos-Kelsey, R., Lu, B., Girman, S., Bischoff, N., Sauve, Y., and Lanza, R. (2006). Human embryonic stem cell-derived cells rescue visual function in dystrophic RCS rats. Cloning Stem Cells 8, 189–199.

Martin, M.J., Muotri, A., Gage, F., and Varki, A. (2005). Human embryonic stem cells express an immunogenic nonhuman sialic acid. Nat. Med. 11, 228–232.

Osakada, F., Jin, Z.B., Hirami, Y., Ikeda, H., Danjyo, T., Watanabe, K., Sasai, Y., and Takahashi, M. (2009). In vitro differentiation of retinal cells from human pluripotent stem cells by small-molecule induction. J. Cell Sci. 122, 3169–3179.

Pennington, B.O., Clegg, D.O., Melkoumian, Z.K., and Hikita, S.T. (2015). Defined culture of human embryonic stem cells and xeno-free derivation of retinal pigmented epithelial cells on a novel, synthetic substrate. Stem Cells Transl. Med. 4, 165–177.

Pinilla, I., Cuenca, N., Martinez-Navarrete, G., Lund, R., and Sauvé, Y. (2009). Intraretinal processing following photoreceptor rescue by non-retinal cells. Vision Res. 49, 2067–2077.

Pittack, C., Grunwald, G.B., and Reh, T.A. (1997). Fibroblast growth factors are necessary for neural retina but not pigmented epithelium differentiation in chick embryos. Development 124, 805–816.

Rodin, S., Antonsson, L., Hovatta, O., and Tryggvason, K. (2014a). Monolayer culturing and cloning of human pluripotent stem cells

on laminin-521-based matrices under xeno-free and chemically defined conditions. Nat. Protoc. *9*, 2354–2368.

Rodin, S., Antonsson, L., Niaudet, C., Simonson, O.E., Salmela, E., Hansson, E.M., Domogatskaya, A., Xiao, Z., Damdimopoulou, P., Sheikhi, M., et al. (2014b). Clonal culturing of human embryonic stem cells on laminin-521/E-cadherin matrix in defined and xeno-free environment. Nat. Commun. *5*, 3195.

Rowland, T.J., Blaschke, A.J., Buchholz, D.E., Hikita, S.T., Johnson, L.V., and Clegg, D.O. (2013). Differentiation of human pluripotent stem cells to retinal pigmented epithelium in defined conditions using purified extracellular matrix proteins. J. Tissue Eng. Regen. Med. *7*, 642–653.

Schwartz, S.D., Hubschman, J.P., Heilwell, G., Franco-Cardenas, V., Pan, C.K., Ostrick, R.M., Mickunas, E., Gay, R., Klimanskaya, I., and Lanza, R. (2012). Embryonic stem cell trials for macular degeneration: a preliminary report. Lancet *379*, 713–720.

Schwartz, S.D., Regillo, C.D., Lam, B.L., Eliott, D., Rosenfeld, P.J., Gregori, N.Z., Hubschman, J.P., Davis, J.L., Heilwell, G., Spirn, M., et al. (2015). Human embryonic stem cell-derived retinal pigment epithelium in patients with age-related macular degener-ation and Stargardt's macular dystrophy: follow-up of two open-label phase 1/2 studies. Lancet *385*, 509–516.

Sparrow, J.R., Hicks, D., and Hamel, C.P. (2010). The retinal pigment epithelium in health and disease. Curr. Mol. Med. *10*, 802–823.

Stanzel, B.V., Liu, Z., Somboonthanakij, S., Wongsawad, W., Brinken, R., Eter, N., Corneo, B., Holz, F.G., Temple, S., Stern, J.H., et al. (2014). Human RPE stem cells grown into polarized RPE monolayers on a polyester matrix are maintained after grafting into rabbit subretinal space. Stem Cell Rep. *2*, 64–77.

Vaajasaari, H., Ilmarinen, T., Juuti-Uusitalo, K., Rajala, K., Onnela, N., Narkilahti, S., Suuronen, R., Hyttinen, J., Uusitalo, H., and Skottman, H. (2011). Toward the defined and xeno-free differenti-ation of functional human pluripotent stem cell-derived retinal pigment epithelial cells. Mol. Vis. *17*, 558–575.

Vugler, A., Carr, A.J., Lawrence, J., Chen, L.L., Burrell, K., Wright, A., Lundh, P., Semo, M., Ahmado, A., Gias, C., et al. (2008). Eluci-dating the phenomenon of HESC-derived RPE: anatomy of cell genesis, expansion and retinal transplantation. Exp. Neurol. *214*, 347–361.